Korean J. Chem. Eng., 37(7), 1206-1211 (2020)
DOI: 10.1007/s11814-020-0548-8

pISSN: 0256-1115
eISSN: 1975-7220

Ethylenediamine-incorporated MIL-101(Cr)-NH_2 metal-organic frameworks for enhanced CO_2 adsorption

The Ky Vo*, Woo-Sik Kim, and Jinsoo Kim**,†**

*Department of Chemical Engineering, Industrial University of Ho Chi Minh City, Ho Chi Minh City, 12 Nguyen Van Bao, Go Vap, Ho Chi Minh City, Vietnam
**Department of Chemical Engineering, Kyung Hee University, 1732 Deogyeong-daero, Giheung-gu, Yongin-si, Gyeonggi-do 17104, Korea
(*Received 7 January 2020 • Revised 11 March 2020 • Accepted 20 March 2020*)

Abstract−Ethylenediamine (EA)-incorporated MIL-101(Cr)-NH_2 adsorbents were prepared for CO_2 adsorption. First, MIL-101(Cr)-NH_2 was directly prepared by the solvothermal method, followed by the EA incorporation inside the pores of MIL-101(Cr)-NH_2. The prepared samples were characterized by N_2 porosimetry, field-emission scanning electron microscopy, transmission electron microscopy, Fourier transform infrared spectrometry, thermogravimetric, and powder X-ray diffraction analyses. The effects of ethylenediamine loading in MIL-101(Cr)-NH_2 on the CO_2 adsorption capability were systematically investigated. EA-incorporated MIL-101(Cr)-NH_2 showed CO_2 adsorption capacity of *ca.* 3.4 mmol/g, which was ~62% higher than the pristine MIL-101(Cr)-NH_2. In addition, the amine-grafted MOF samples showed good regenerability and stability after consecutive adsorption-desorption cycles at ambient conditions. These suggest that introduction of alkylamine molecules into the pores of metal-organic frameworks can be a promising strategy to improve the CO_2 soprtion ability of MOFs.

Keywords: MOFs, MIL-101(Cr)-NH_2, Ethylenediamine@MIL-101(Cr)-NH_2, CO_2 Adsorption

INTRODUCTION

The development of efficient strategies to mitigate CO_2 emission has gained considerable attention [2,3,13]. Recently, large-scale adsorption of CO_2 from industrial streams has been widely performed using amine-based solutions. However, these solutions have low capacity problems at very dilute CO_2 concentrations and high heat capacity, which makes the regeneration very energy intensive [18]. However, amine-functionalized solid adsorbents have emerged as promising candidates for CO_2 adsorption owing to their lower heat capacity. Instead, amine-doped zeolite and silica adsorbents have been successfully synthesized with excellent selectivity for CO_2 adsorption and low heat capacity [1,7,11]. However, the CO_2 adsorption capability of these solid adsorbents is still low owing to their low porosity. Therefore, it is still essential to develop porous materials with high porosity and suitable pore sizes to produce amine-incorporated adsorbents with a high CO_2 adsorption capacity.

Metal-organic frameworks (MOFs) have been considered as promising materials for CO_2 capture owing to their high surface area, large pore volume, and tunable pore structure [5,21,23]. However, several aspects need to be carefully evaluated for the use of MOFs as adsorbent materials for CO_2 adsorption from flue gas or natural gas upgrading owing to the chemical and thermal stabilities of MOFs in addition to CO_2 adsorption capacity and selectivity. It has been reported that many MOFs are extremely sensitive to moisture or are hydrolytically unstable, which limits their practical applications [17]. For instance, MOF-74(Mg) was discovered to have a high CO_2 uptake capacity; however, it has a relatively low water stability [4]. Therefore, a promising material for CO_2 capture should possess not only the ultrahigh adsorption capacity but also high stability.

To improve CO_2 capturing using MOFs, there are some strategies that are usually used, such as chemical functionalization [2,20], incorporation of unsaturated metal cation centers [28], metal doping [21], or synthesis of MOF-based composite materials [3]. Among them, the incorporation of amine functionalities into the pores of MOFs has received considerable attention for increasing both the CO_2 uptake amount and its selectivity. The incorporation of polyethyleneimine into MIL-101(Cr) or amine-MIL-101(Cr) frameworks resulted in an enhanced CO_2 adsorption capacity and CO_2 selectivity [16,26]. Lee et al. [12] incorporated ethylenediamine into the Mg_2(dopdc) framework, which showed an isosteric heat of adsorption for CO_2 capture of 49-51 kJ mol^{-1} and an enhanced CO_2 adsorption capacity. Grafting of N,N′-dimethylethylenediamine molecules onto coordinatively unsaturated Cu^{2+} sites of the CuBTTri framework induced a drastically enhanced CO_2 adsorption at low concentration and exceptionally large isosteric heat of CO_2 adsorption of 96 kJ mol^{-1} [19]. Very recently, Zhong et al. [27] prepared amine-grafted MIL-101(Cr) samples using tris(2-aminoethyl) amine (TAEA), ethylenediamine (ED), and triethylene diamine (TEDA). Zhong et al. determined that the ED@MIL-101(Cr) and TAEA@MIL-101(Cr) samples showed enhanced CO_2 capture capacity, which corresponded to their enhanced isosteric enthalpy for CO_2 adsorption [27]. However, Kim et al. [10] reported that grafting diethylen-

†To whom correspondence should be addressed.
E-mail: jkim21@khu.ac.kr

etriamine molecules within the pores of MIL-101(Cr) decreased the CO_2 capture capacity compared to that of pristine MOF. This suggests that additional investigations are needed to study these promising materials before bringing them into industrial applications. For amine-grafted adsorbents, one of the amine groups can be grafted onto the coordinatively unsaturated cationic site (CUS), while other amine groups remain available as chemically reactive adsorption sites owing to the affinity of amines for CO_2 molecules, which enhances the CO_2 adsorption [2,12]. Therefore, various parameters (e.g., the concentration and structure of amine, as well as the porosity and particle size of MOF) should be carefully optimized to achieve the best CO_2 selective material [16].

In this study, ethylenediamine(EA)-incorporated MIL-101(Cr)-NH_2 adsorbents were prepared with different amine concentrations. To our knowledge, there are no reports on EA-incorporated MIL-101(Cr)-NH_2 adsorbent for CO_2 adsorption. MIL-101(Cr)-NH_2 was chosen because its three-dimensional network is formed from amine-based bridging ligands, which can enhance the CO_2 capturing ability. In addition, MIL-101(Cr)-NH_2 was observed to have a good moisture-resistant stability, which is crucial for its practical applications [14,15]. Then, the prepared EA@MIL-101(Cr)-NH_2 adsorbents were tested for CO_2 adsorption at different temperatures. The heat of CO_2 adsorption on pure MIL-101(Cr)-NH_2 and EA@MIL-101(Cr)-NH_2 samples was compared. In addition, consecutive adsorption-desorption cycles were performed to evaluate the regenerability of amine-grafted samples.

EXPERIMENTAL

1. Synthesis of MIL-101(Cr)-NH_2 and EA-incorporated MIL-101(Cr)-NH_2

MIL-101(Cr)-NH_2 was directly prepared by solvothermal synthesis. Typically, 1.6 g of $Cr(NO_3)_3{\cdot}9H_2O$ (4 mmol; Sigma-Aldrich, 99%) and 0.72 g of 2-aminoterephthalic acid (4 mmol; Sigma-Aldrich, 99%) were dispersed in 25 mL of deionized water under stirring. Then, the mixture was sonicated for 10 min before being transferred to a 50-mL Teflon-lined stainless steel autoclave and maintained at 150 °C for 24 h. The reaction mixture was then cooled to ambient temperature. The green product was collected and repeatedly washed with DMF (2 times) and EtOH (2 times) at 70 °C for 6 h. The obtained solids were finally dried at 80 °C in air for 12 h. The prepared samples were activated at 150 °C for 12 h under vacuum before the adsorption test.

The incorporation of EA into MIL-101(Cr)-NH_2 was conducted according to the previously reported procedure [8] with a slight modification. Typically, a certain amount of EA was dissolved in 35 mL of anhydrous hexane (99.5%, Sigma-Aldrich) under stirring using a three-neck flask. To this solution, 1.5 g of activated MIL-101(Cr)-NH_2 was added slowly under stirring. The mixture was refluxed under N_2 atmosphere for 12 h to achieve amine grafting. The resulting mixture was filtered and washed several times with anhydrous hexane. The obtained solid was dried overnight at room temperature under vacuum to obtain the final product. The product was denoted as *n*EA@MIL-101(Cr)-NH_2, in which *n* is the weight percentage of EA incorporated into MOF ($n=m_{EA}/(m_{EA}+m_{MOF})\times100\%$). To calculate the accurate amount of amine loading, the masses of MIL-101(Cr)-NH_2 and EA@MIL-101(Cr)-NH_2 were weighed immediately after degassing.

2. Characterization

The morphology of the prepared MIL-101(Cr)-NH_2 and EA@MIL-101(Cr)-NH_2 samples was examined using field-emission scanning electron microscopy (FE-SEM; Leo-Supra 55, Carl Zeiss STM, Germany). The N_2 adsorption-desorption isotherms of the samples were measured at 77 K after degassing at 423 K for 12 h using N_2 porosimetry (BELSORP-max, BEL, Japan). The FT-IR analyses were conducted in the range of 4,000-400 cm^{-1} using an FT-IR spectrometer (Tensor 27, Bruker, Germany). The crystallographic structures of the prepared MIL-101(Cr)-NH_2 and EA@MIL-101(Cr)-NH_2 samples were determined using powder X-ray diffraction (XRD; MAC-18XHF, Rigaku, Japan). The thermal stability of the synthesized MIL-101(Cr)-NH_2 was examined by a thermogravimetric analyzer (Q50, TA Instruments, USA) under N_2 gas at a heating rate of 5 °C/min.

3. Gas Adsorption

CO_2 adsorption isotherms of the samples were measured by an adsorption analyzer (BELSORP-mini II, Bel, Japan) under pressures up to 100 kPa by means of a standard static volumetric technique. The adsorption temperature was strictly monitored using a thermostatic bath connected to a vacuum flask with a circulating jacket. Typically, 0.6 g of the adsorbent was activated at 90 °C for 2 h under vacuum (10^{-2} kPa) and then cooled to room temperature before the adsorption of CO_2 (99.99%) at designed temperature.

RESULTS AND DISCUSSION

1. Characteristics of MIL-101(Cr)-NH_2 and EA@MIL-101(Cr)-NH_2

The thermal stability of the prepared MIL-101(Cr)-NH_2 was examined by TGA, which indicated that MIL-101(Cr)-NH_2 was stable up to ~270 °C (Fig. S1), in agreement with the previous report

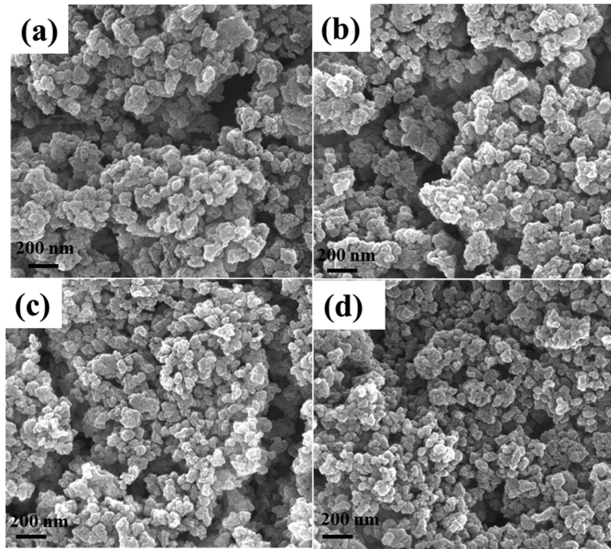

Fig. 1. SEM images of (a) MIL-101(Cr)-NH_2, (b) 9.1EA@MIL-101(Cr)-NH_2, (c) 32.6EA@MIL-101(Cr)-NH_2, and (d) 39.5EA@MIL-101(Cr)-NH_2.

[15]. The morphologies of the prepared MIL-101(Cr)-NH_2 and EA-incorporated MIL-101(Cr)-NH_2 samples are shown in Fig. 1. The SEM image of pure MIL-101(Cr)-NH_2 shows the formation of aggregated spheroidal-shaped nanoparticles. The morphology of the EA@MIL-101(Cr)-NH_2 samples was similar to that of parent MOF, which suggests that the incorporation of EA molecules into the pores of MOF structure did not change their morphology. The TEM analyses of MIL-101(Cr)-NH_2 and EA@MIL-101(Cr)-NH_2 revealed that these nanoparticles were highly aggregated with the particle size in the range of 20-100 nm [Figs. S2(a), (b)].

Fig. 2 shows the XRD patterns of the prepared samples. The XRD pattern of MIL-101(Cr)-NH_2 showed the same topological structure of the MIL-101(Cr)-NH_2 reported in the literature [6,15, 22]. The broad XRD peaks of the amine-functionalized MIL-101(Cr)-NH_2 samples suggest smaller crystallite sizes, which is consistent with the data of SEM and TEM analyses. It was observed that the introduction of EA molecules into the MOF framework resulted in a decrease in the XRD peak intensities. In addition, the diffraction peaks of the EA@MIL-101(Cr)-NH_2 samples shifted to lower angles compared to those of parent MIL-101(Cr)-NH_2. This result was obtained owing to the loading of amine molecules into the pores of the MIL-101(Cr)-NH_2 frameworks.

Fig. 3 shows the FT-IR spectra of the pure MIL-101(Cr)-NH_2 and EA@MIL-101(Cr)-NH_2 samples. The incorporation of amines was confirmed by an increase in the bands at 3,490 cm^{-1} and 3,380 cm^{-1} that appeared for the EA@MIL-101(Cr)-NH_2 samples; the abovementioned bands correspond to asymmetric and symmetric stretches of the amine moieties, respectively [15]. The methylene groups of amines on EA-incorporated samples resulted in the presence of a doublet at 2,945 cm^{-1} (asymmetric CH_2 stretch) and 2,840 cm^{-1} (symmetric CH_2 stretch) [10]. The vibrational modes at 1,624 cm^{-1} and 1,586 cm^{-1} are ascribed to the bending of N-H. The peaks at 1,256 cm^{-1} and 1,338 cm^{-1} are assigned to the stretching of the C-N bond of aromatic amines [9,15]. These vibration bands are strong in the IR spectrum of pristine MIL-101(Cr)-NH_2 but weak in the FT-IR spectrum of EA@MIL-101(Cr)-NH_2 samples. The bands at approximately 1,070 cm^{-1} are attributed to the C-N stretching vibration of aliphatic amines [9], which appeared only in the IR spectra of the EA@MIL-101(Cr)-NH_2 samples owing

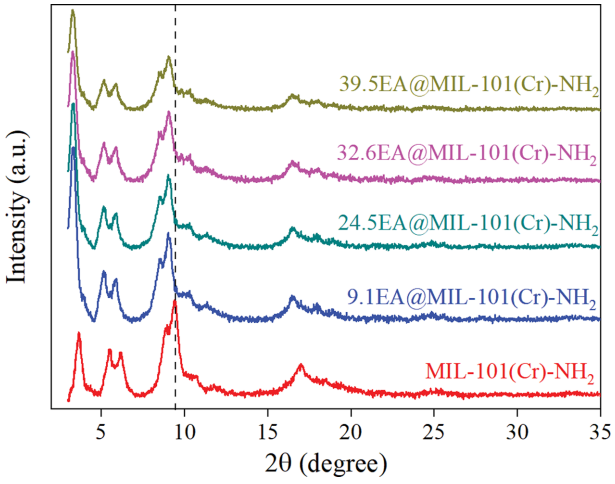

Fig. 2. XRD patterns of pristine MIL-101(Cr)-NH_2 and EA@MIL-101(Cr)-NH_2 samples.

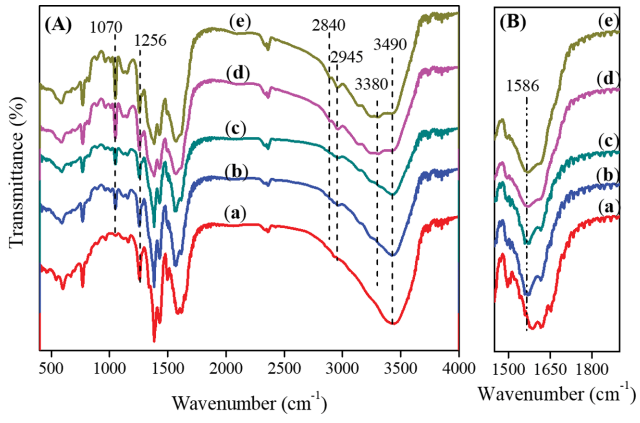

Fig. 3 (A) and (B) FT-IR spectra of (a) MIL-101(Cr)-NH_2, (b) 9.1EA@MIL-101(Cr)-NH_2, (c) 21.5EA@MIL-101(Cr)-NH_2, (d) 32.6EA@MIL-101(Cr)-NH_2, and (e) 39.5EA@MIL-101(Cr)-NH_2.

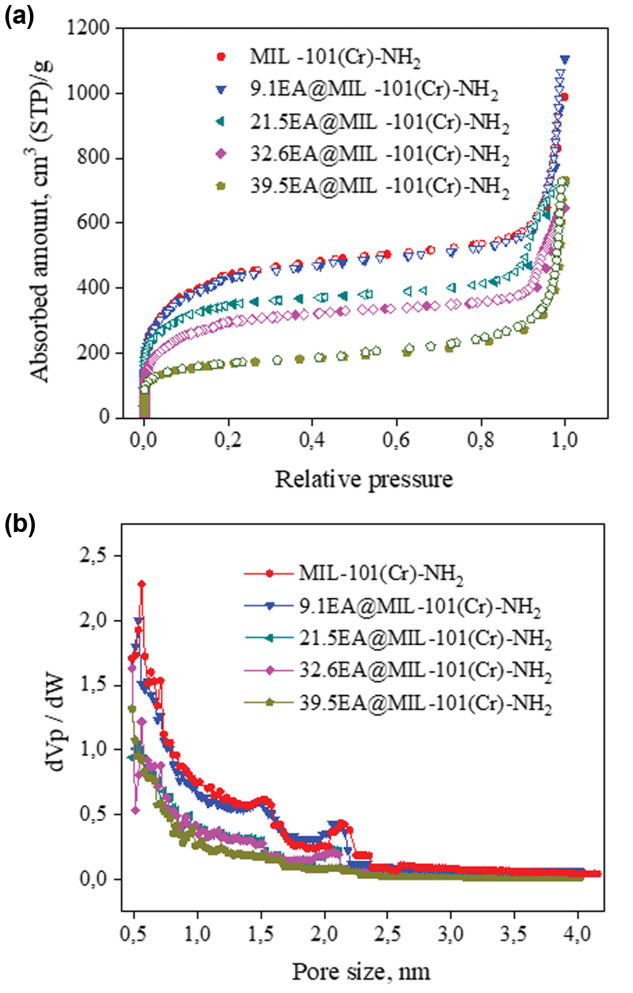

Fig. 4. Textural properties of the prepared adsorbents: (a) N_2 adsorption-desorption isotherms, and (b) pore size distributions.

Table 1. Textural properties of the MIL-101(Cr)-NH_2 and EA@MIL-101(Cr)-NH_2 samples

Sample	EA loading wt%	S_{BET} $m^2 \cdot g^{-1}$	Total pore volume, $cm^3 \cdot g^{-1}$
MIL-101(Cr)-NH_2	-	1,720	1.54
9.1EA@MIL-101(Cr)-NH_2	9.1	1,598	1.41
21.5EA@MIL-101(Cr)-NH_2	21.5	1,183	1.09
32.6EA@MIL-101(Cr)-NH_2	32.6	980	0.97
39.5EA@MIL-101(Cr)-NH_2	39.5	605	0.64

to the loading of EA. In addition, the peak at 1,586 cm^{-1} in the FT-IR spectra of EA-doped samples slightly shifted compared to that in the FT-IR spectrum of pristine MOF [see Fig. 3(B)] owing to the coordination of amines onto CUS Cr(III). These results confirm that EA molecules were successfully introduced into the MIL-101(Cr)-NH_2 frameworks.

The N_2 adsorption-desorption isotherms and pore size distributions of the prepared samples are shown in Figs. 4(a)-(b). As shown in Fig. 4(a), the parent MIL-101(Cr)-NH_2 and EA@ MIL-101(Cr)-NH_2 samples exhibit typical type I isotherms. The high nitrogen uptake at a very low relative pressure demonstrates that MIL-101(Cr)-NH_2 contains micropores, which is consistent with the previous reports on the textural properties of MIL-101(Cr)-NH_2 [15,25]. The introduction of EA molecules into MIL-101(Cr)-NH_2 resulted in a decrease in the N_2 uptake capacity [Fig. 4(a)]. This may be attributed to the loaded amine molecules obstructing N_2 diffusion as well as the partial occupation of the space inside the pores [2]. Table 1 shows the BET surface areas and total pore volumes of the MIL-101(Cr)-NH_2 and EA@MIL-101(Cr)-NH_2 samples. Pristine MIL-101(Cr)-NH_2 possess the BET surface area and pore volume of 1,720 $m^2\ g^{-1}$ and 1.54 $cm^3\ g^{-1}$, respectively. The incorporation of EA gradually decreased the surface area and total pore volume. Specifically, with an increase in the loading amount of EA from 9.1 wt% to 39.5 wt%, the BET surface area and total pore volume decreased from 1,598 $m^2\ g^{-1}$ to 605 $m^2\ g^{-1}$ and from 1.41 $cm^3\ g^{-1}$ to 0.74 $cm^3\ g^{-1}$, respectively.

2. CO_2 Adsorption Test

Fig. 5 shows the CO_2 adsorption capacity of the parent MIL-101(Cr)-NH_2 and EA@MIL-101(Cr)-NH_2 samples at 25 °C in the pressure range of 0-100 kPa. At 100 kPa, MIL-101(Cr)-NH_2 exhibited the CO_2 adsorption capacity of 2.10 $mmol \cdot g^{-1}$, which is comparable to that previously reported for MIL-101(Cr)-NH_2 [15]. With an increase in the EA loading to 9.1, 21.5, and 32.6 wt% on MIL-101(Cr)-NH_2, the CO_2 adsorption capacity increased to 2.5, 2.80, and 3.4 $mmol \cdot g^{-1}$, respectively. This indicates that the incorporation of amine groups into MIL-101(Cr)-NH_2 frameworks enhanced the CO_2 capture ability of the adsorbents, which is attributed to the introduction of additional CO_2 affinity sites. It has been re-

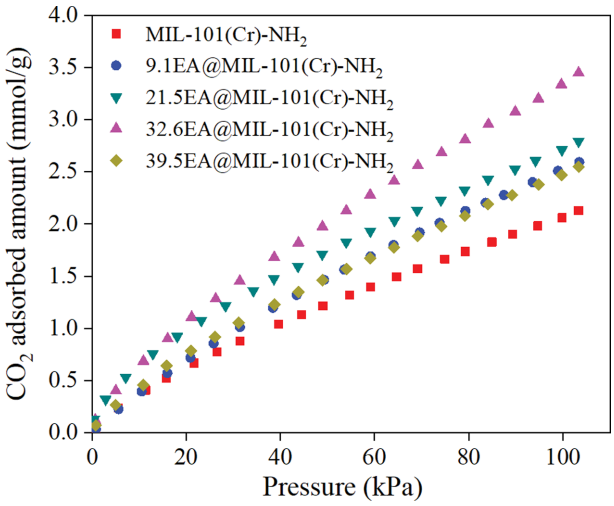

Fig. 5. CO_2 adsorption isotherms of pristine MIL-101(Cr)-NH_2 and EA@MIL-101(Cr)-NH_2 samples at 25 °C.

Table 2. Comparison of the CO_2 capture capacity of the amine-incorporated MOF adsorbents

Adsorbent	CO_2 capture capacity (mmol/g) at 25 °C and 100 kPa	Ref.
Ethylendiamine@MIL-101(Cr)-NH_2	3.4	This work
Diethylenetriamine@MIL-101(Cr)	0.7	[10]
Ethylenediamine@MIL-101(Cr)	1.9	[27]
Tris(2-aminoethyl) amine@MIL-101(Cr)	2.2	[27]
Triethylene diamine@MIL-101(Cr)	1.7	[27]
Ethylenediamine@MIL-100(Cr)(*)	2.4	[2]
N,N′-dimethylethylenediamine@MIL-100(Cr)(*)	1.7	[2]
PEI@MIL-101(Cr)-NH_2	3.6	[26]
PEI@MIL-101(Cr)	3.7	[16]

(*) 35 °C

ported that there is a chemisorption interaction between CO_2 and amine sites, which facilitates CO_2 sorption and CO_2 co-adsorption into the MOF framework [2,12,19]. However, it has been observed that the incorporation of a higher amine amount (39.5 wt%) decreased the CO_2 uptake capacity (Fig. 5). This result is due to the rapid decrease in the surface area and pore volume of the adsorbent; the excess amount of amines blocked the pores and slowed diffusion rates of the gaseous molecules. In this study, the highest CO_2 capture capacity of 3.4 mmol·g^{-1} was obtained for the 32.6EA@MIL-101(Cr)-NH_2 sample, which was comparable to that of PEI@MIL-101(Cr) and higher than that of ethylenediamine@MIL-100(Cr), tris(2-aminoethyl)amine@MIL-101(Cr), triethylenediamine@MIL-101(Cr), or diethylenetriamine@MIL-101(Cr), as summarized in Table 2.

Fig. 6 shows the CO_2 adsorption capacity on the 32.6EA@MIL-101(Cr)-NH_2 adsorbent at different temperatures. As expected, the CO_2 capture capacity decreased with an increase in the temperature, which suggests the exothermic nature of the gas adsorption process on the 32.6EA@MIL-101(Cr)-NH_2 sample. The obtained CO_2 adsorption isotherm data for MIL-101(Cr)-NH_2 and 32.6EA@MIL-101(Cr)-NH_2 at different temperatures were fitted with adsorption models to obtain the exact pressures corresponding to the adsorbed CO_2 quantities. Specifically, the dual-site Langmuir-Freundlich model showed the best fit. Then, the obtained data were utilized to estimate the isosteric heats of adsorption using the Clausius-Clapeyron equation [12,24]:

$$\ln(p)_q = \left(\frac{-\Delta H}{R}\right)\left(\frac{1}{T}\right) + C \quad (1)$$

where p is the pressure, R is the ideal gas constant, T is the absolute temperature and C is the constant. Therefore, ΔH can be derived from the slopes of plots of lnp versus 1/T.

Fig. 7 shows the isosteric heats of CO_2 adsorption on both MIL-101(Cr)-NH_2 and 32.6EA@MIL-101(Cr)-NH_2 samples as a function of the CO_2 uptake amount. At low coverage, the heat of adsorption on parent MIL-101(Cr)-NH_2 was calculated to be ca. 43 kJ mol^{-1}, which is in agreement with the previously published data [15]. Meanwhile, the initial isosteric heat of CO_2 adsorption on 32.6EA@MIL-101(Cr)-NH_2 was ca. 83 kJ mol^{-1}, which is much higher than that on the pristine MIL-101(Cr)-NH_2. This implies

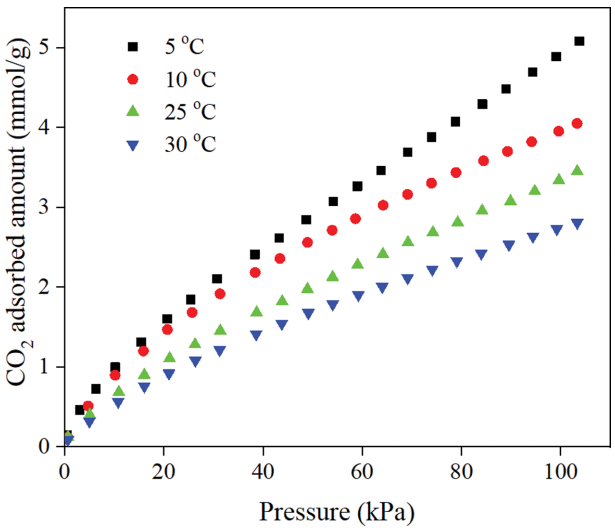

Fig. 6. CO_2 adsorption isotherms on 32.6EA@MIL-101(Cr)-NH_2 sample at different temperatures.

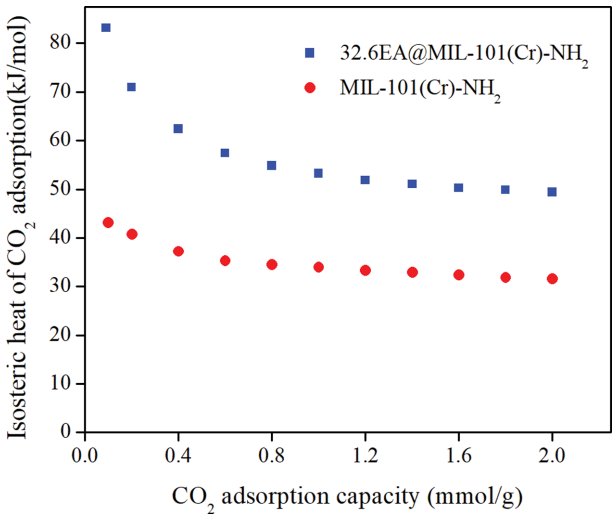

Fig. 7. Isosteric heats of CO_2 adsorption on pure MIL-101(Cr)-NH_2 and 32.6EA@MIL-101(Cr)-NH_2 samples.

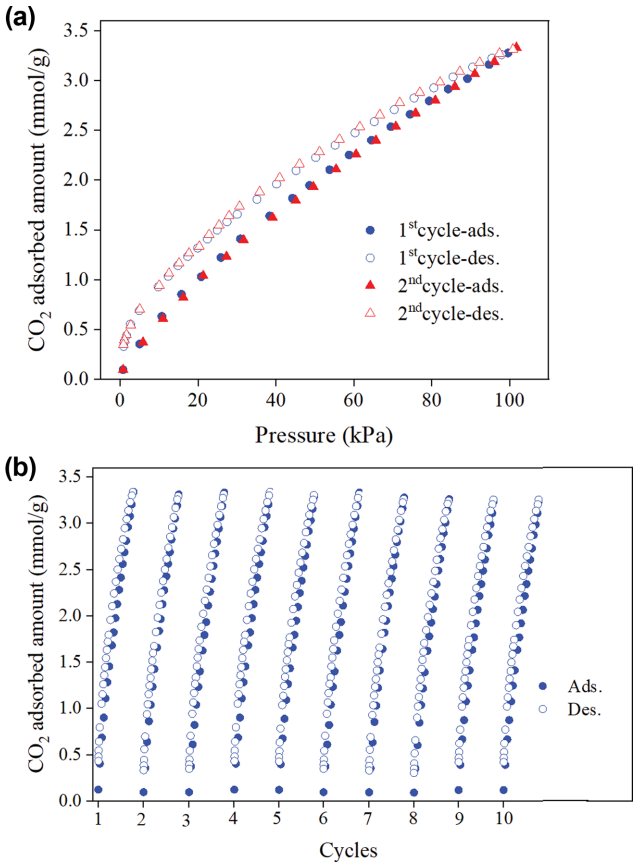

Fig. 8. Regeneration tests on the 32.6EA@MIL-101(Cr)-NH_2 sample after the (a) first and second cycle and after (b) ten cycles.

that 32.6EA@MIL-101(Cr)-NH_2 interacted more strongly with CO_2 than pure MIL-101(Cr)-NH_2, which suggests the strong and selective interaction of CO_2 molecules with the alkylamine functionalities [2,12,19]. This result was obtained because EA grafted on the MIL-101(Cr)-NH_2 operates as a Lewis base, which can adsorb acidic CO_2 molecules more strongly than the Lewis acid CUS Cr(III) of parent MOF by promoting the formation of a carbamate-like complex [10,12].

3. Regeneration of the Adsorbent

Regenerability tests were performed to evaluate the reusability of the prepared adsorbents. A series of CO_2 adsorption and desorption isotherms were obtained for the 32.6EA@MIL-101(Cr)-NH_2 sample at 25 °C. After each CO_2 adsorption-desorption cycle, the adsorbent was treated by heating to 90 °C under vacuum for 2 h before using it as a regenerated sample. Fig. 8(a) shows the adsorption-desorption isotherms of CO_2 for the first and second cycles. It was observed that a small hysteresis between the adsorption and desorption curves existed, and the desorption of CO_2 was incomplete under the designed conditions, which indicates that harsher conditions are needed to completely regenerate the adsorbent [2]. After ten adsorption-desorption cycles, the total CO_2 capture capacity of the EA-grafted sample is approximately 95% of its maximum capture capacity [Fig. 8(b)], which shows a very small capacity loss.

CONCLUSIONS

EA-grafted MIL-101(Cr)-NH_2 adsorbents were prepared with different amine concentrations. The incorporation of EA molecules within the pores of the MIL-101(Cr)-NH_2 framework resulted in an increased CO_2 capture capacity owing to the introduction of additional CO_2 affinity sites even though the surface area and pore volume of the adsorbent decreased. The highest CO_2 adsorption capacity of 3.4 mmol/g was obtained over the 32.6EA@MIL-101(Cr)-NH_2 sample, which is approximately 62% higher than that of parent MOF. The heat of CO_2 adsorption on the amine-grafted sample was ca. 83 kJ/mol, which is almost two-times higher than that on pristine MOF at low coverage. Furthermore, after 10 adsorption-desorption cycles at ambient conditions, the CO_2 capacity loss was very small (~5%). This suggests that the EA@MIL-101(Cr)-NH_2 adsorbent is a promising material for CO_2 capture.

ACKNOWLEDGEMENTS

This work was supported by the Industrial University of Ho Chi Minh City, Vietnam (19.2H02), the Basic Science Research Program (NRF-2019R1A2C1090693) and the Engineering Research Center of Excellence Program (NRF-2014R1A5A1009799) through the National Research Foundation (NRF) funded by the Ministry of Science and ICT, Republic of Korea.

SUPPORTING INFORMATION

Additional information as noted in the text. This information is available via the Internet at http://www.springer.com/chemistry/journal/11814.

REFERENCES

1. Y. Belmabkhout, R. Serna-Guerrero and A. Sayari, *Adsorption*, **17**, 395 (2011).
2. C. P. Cabello, G. Berlier, G. Magnacca, P. Rumori and G. T. Palomino, *CrystEngComm.*, **17**, 430 (2015).
3. Y. Cao, Y. Zhao, Z. Lv, F. Song and Q. Zhong, *J. Ind. Eng. Chem.*, **27**, 102 (2015).
4. J. B. DeCoste, G. W. Peterson, B. J. Schindler, K. L. Killops, M. A. Browe and J. J. Mahle, *J. Mater. Chem. A.*, **1**, 11922 (2013).
5. P. D. C. Dietzel, V. Besikiotis and R. Blom, *J. Mater. Chem.*, **19**, 7362 (2009).
6. A. T. E. Vilian, B. Dinesh, R. Muruganantham, S. R. Choe, S.-M. Kang, Y. S. Huh and Y.-K. Han, *Microchim. Acta*, **184**, 4793 (2017).
7. A. Goeppert, M. Czaun, R. B. May, G. K. S. Prakash, G. A. Olah and S. R. Narayanan, *JACS*, **133**, 20164 (2011).
8. Y. K. Hwang, D.-Y. Hong, J.-S. Chang, S. H. Jhung, Y.-K. Seo, J. Kim, A. Vimont, M. Daturi, C. Serre and G. Férey, *Angew. Chem. Int. Ed.*, **47**, 4144 (2008).
9. N. Janakiraman and M. Johnson, *Rom. J. Biophys.*, **25**, 131 (2015).
10. S.-N. Kim, S.-T. Yang, J. Kim, J.-E. Park and W.-S. Ahn, *CrystEngComm.*, **14**, 4142 (2012).
11. Y. Kuwahara, D.-Y. Kang, J. R. Copeland, N. A. Brunelli, S. A. Didas, P. Bollini, C. Sievers, T. Kamegawa, H. Yamashita and C. W. Jones, *JACS*, **134**, 10757 (2012).
12. W. R. Lee, S. Y. Hwang, D. W. Ryu, K. S. Lim, S. S. Han, D. Moon, J. Choi and C. S. Hong, *Energy Environ. Sci.*, **7**, 744 (2014).
13. J.-R. Li, R. J. Kuppler and H.-C. Zhou, *Chem. Soc. Rev.*, **38**, 1477 (2009).
14. N. Li, J. Xu, R. Feng, T.-L. Hu and X.-H. Bu, *Chem. Commun.*, **52**, 8501 (2016).
15. Y. Lin, C. Kong and L. Chen, *RSC Adv.*, **2**, 6417 (2012).
16. Y. Lin, H. Lin, H. Wang, Y. Suo, B. Li, C. Kong and L. Chen, *J. Mater. Chem. A.*, **2**, 14658 (2014).
17. J. Liu, P. K. Thallapally, B. P. McGrail, D. R. Brown and J. Liu, *Chem. Soc. Rev.*, **41**, 2308 (2012).
18. X. Ma, X. Wang and C. Song, *JACS*, **131**, 5777 (2009).
19. T. M. McDonald, D. M. D'Alessandro, R. Krishna and J. R. Long, *Chem. Sci.*, **2**, 2022 (2011).
20. L. Mei, T. Jiang, X. Zhou, Y. Li, H. Wang and Z. Li, *Chem. Eng. J.*, **321**, 600 (2017).
21. H. J. Park and M. P. Suh, *Chem. Sci.*, **4**, 685 (2013).
22. M. Saikia and L. Saikia, *RSC Adv.*, **6**, 14937 (2016).
23. A. Schneemann, S. Henke, I. Schwedler and R. A. Fischer, *ChemPhysChem.*, **15**, 823 (2014).
24. T. K. Vo, Y.-S. Bae, B.-J. Chang, S.-Y. Moon, J.-H. Kim and J. Kim, *Micropor. Mesopor. Mater.*, **274**, 17 (2019).
25. M. Wen, K. Mori, T. Kamegawa and H. Yamashita, *Chem. Commun.*, **50**, 11645 (2014).
26. Q. Yan, Y. Lin, C. Kong and L. Chen, *Chem. Commun.*, **49**, 6873 (2013).
27. R. Zhong, X. Yu, W. Meng, J. Liu, C. Zhi and R. Zou, *ACS Sustain. Chem. Eng.*, **6**, 16493 (2018).
28. Z. Zhou, L. Mei, C. Ma, F. Xu, J. Xiao, Q. Xia and Z. Li, *Chem. Eng. Sci.*, **147**, 109 (2016).

Supporting Information

Ethylenediamine-incorporated MIL-101(Cr)-NH_2 metal-organic frameworks for enhanced CO_2 adsorption

The Ky Vo*, Woo-Sik Kim, and Jinsoo Kim**,†**

*Department of Chemical Engineering, Industrial University of Ho Chi Minh City, Ho Chi Minh City, 12 Nguyen Van Bao, Go Vap, Ho Chi Minh City, Vietnam
**Department of Chemical Engineering, Kyung Hee University, 1732 Deogyeong-daero, Giheung-gu, Yongin-si, Gyeonggi-do 17104, Korea
(*Received 7 January 2020 • Revised 11 March 2020 • Accepted 20 March 2020*)

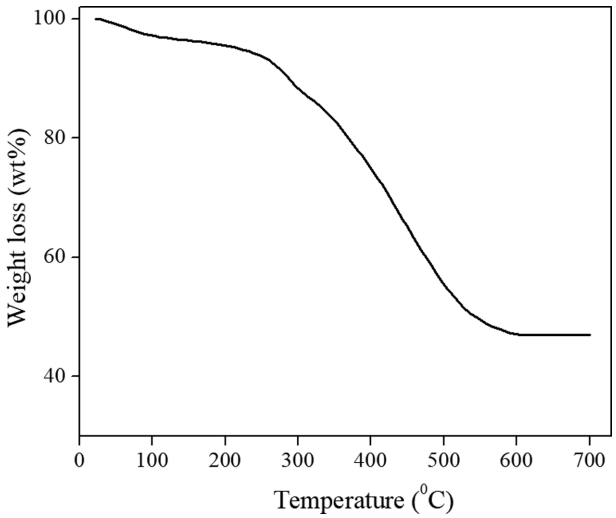

Fig. S1. TGA analysis of MIL-101(Cr)-NH_2 under nitrogen gas at a heating rate of 5 °C·min^{-1}.

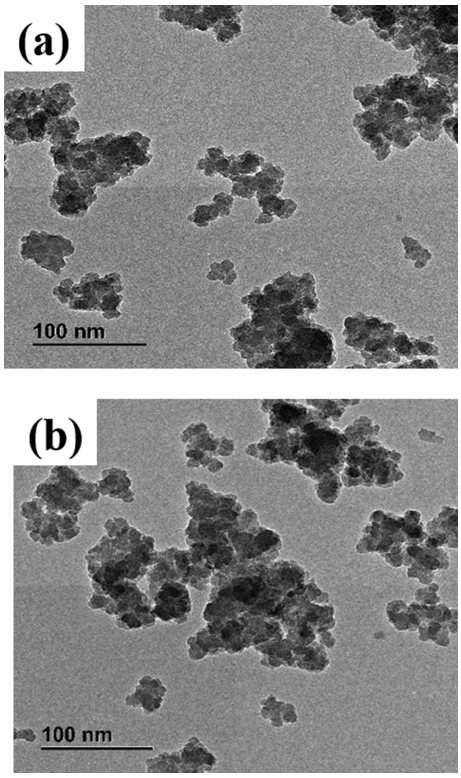

Fig. S2. TEM images of (a) MIL-101(Cr)-NH_2 and (b) 32.6EA@MIL-101(Cr)-NH_2.